Electrochemistry of metal adlayers on metal chalcogenides

G.A. Ragoisha[1*], Y.M. Aniskevich[1,2], A.S. Bakavets[1,2], E.A. Streltsov[2]

[1]Research Institute for Physical Chemical Problems, Belarusian State University, 220006 Minsk, Belarus

[*]ragoisha@yahoo.com

[2]Belarusian State University, Nezalezhnastsi Av. 4, 220030 Minsk, Belarus

Abstract Electrodeposition of metal adlayers on semiconductor metal chalcogenides (CdSe, CdS, PbTe, PbSe, PbS, Bi_2Te_3) is reviewed. Cathodic underpotential deposition of metal adlayer on metal chalcogenide is the electrochemically irreversible surface limited reaction. The irreversibility of the upd increases in the row from tellurides to selenides and further to sulfides. The underpotential shift on chalcogenide nanoparticles increases with particle size. Metal upd on chalcogenides is applied as a means of measurement of electroactive surface area of chalcogenide electrodes. The method is especially advantageous for multicomponent systems with other component not supporting upd, such as $CdSe-TiO_2$, CdSe-ZnO. Differences of voltammetric profiles of Pb upd on Bi_2Te_3 and Te are applied for detection of Bi_2Te_3 surface contamination by elemental tellurium. The further tasks in the electrochemistry of metal adlayers are their incorporation as interlayers in layered chalcogenides and electrodeposition of superlattices.

Introduction

Electrodeposition of a metal atomic layer (adlayer) on a foreign substrate proceeds under thermodynamic conditions different from those of the electrodeposition on the same metal substrate. The difference which results from effect of substrate is characterized by the 'underpotential shift' ΔE_{upd} of the adlayer deposition potential vs. corresponding Nernst potential $E(Me^{n+}/Me_{bulk})$, where Me_{bulk} is bulk metal. Underpotential deposition (upd) of metal adlayers on metals and their anodic oxidation have been comprehensively reviewed [1–7], a less elucidated is the electrochemistry of metal adlayers on nonmetals, such as chalcogens [8, 9], while the electrochemistry of metal adlayers on metal chalcogenides misses review literature, despite great significance of metal adatoms, submonolayers and adlayers as intermediates in electrodeposition of metal chalcogenides [10] and the lately developed electrodeposition of metal-metal chalcogenide superlattice structures [11]. Metal adlayer on semiconductor metal chalcogenide is also an interesting probe object for characterization of size dependences of physical and physicochemical properties of semiconductor nanoparticles [12, 13].

Due to correlations of underpotential shift with the semiconductor nanoparticle size, the routine measurement of quantum dot (QD) size by optical spectroscopy may be substituted by measurement of underpotential shift [12], when in situ optical measurement is less convenient, e.g. in multicomponent nanostructured systems. Selectivity of metal adlayer electrodeposition on metal chalcogenide components of chalcogenide-oxide heterostructures is also a useful feature which allows measurement of electroactive surface area of the chalcogenide spectral sensitizer in the sensitized wide bandgap metal oxide photoanodes [14].

The electrochemistry of metal adlayers on chalcogenides has been applied in works dedicated to layer-by-layer electrochemical assembly of metal chalcogenide materials [15–23]. However, most of the works present electrochemistry just of initial steps of chalcogenide assembly. This minireview is based on own research of the authors with the focus on the results published in the last five years.

Cyclic voltammetry and frequency response

Electrochemical methods are very powerful in general as a means of analysis of solids [24, 25], and the metal adlayers on metal chalcogenides are very characteristic examples of solid state electrochemistry objects which depend critically on electroanalytical methods. Especially complicated for nonelectrochemical analysis are the metal adlayers on the chalcogenides of the same metal (Pb_{ad}-PbTe, Cd_{ad}-CdSe, etc.), as they differ just in the easily mutable chemical state from metal atoms of the substrate and this determines the use of highly sensitive electrochemical techniques for characterization of the electrochemically generated adlayers.

The upd, as well as the anodic oxidation of the electrodeposited adlayer, is surface limited reaction which fades fast at a fixed potential, so the analytical current in stationary voltammetry is equal to zero. For this reason, potentiodynamic rather than stationary versions of voltammetry and impedance spectroscopy were used for electrochemical characterization of the adlayers. While the advantage of cyclic voltammetry (CV) is self-evident, minor explanation may be required for the use of potentiodynamic instead of stationary impedance spectroscopy for frequency response analysis of the cathodic deposition and anodic oxidation of adlayers.
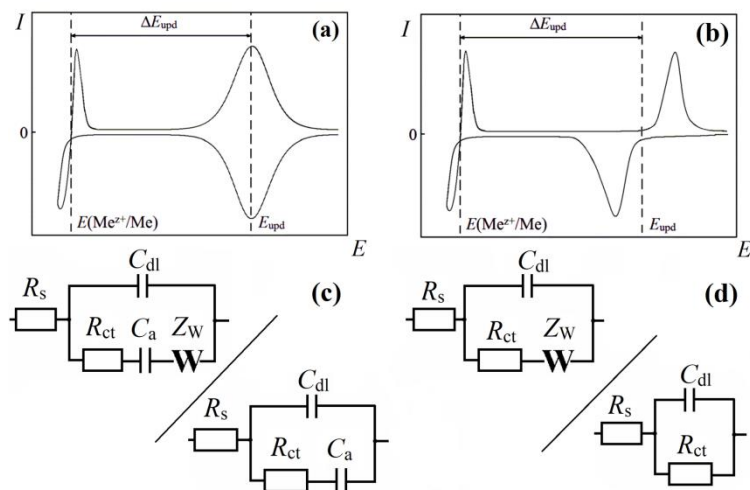
Fig.1 Typical CVs at (a) electrochemically reversible and (b) electrochemically irreversible upd behavior and (c, d) the corresponding equivalent electric circuits applicable in the potential regions of the adlayer cathodic deposition and anodic oxidation

Figure 1 shows two limiting cases of potentiodynamic voltammetric profiles of upd with the corresponding equivalent electric circuits derived from impedance spectroscopy. A pair of perfectly reversible surface limited reactions (the cathodic deposition and the anodic oxidation of an adlayer) gives mirror symmetric cathodic and anodic peaks (Fig.1a), while electrochemical irreversibility of upd results in the separation of the cathodic and anodic peaks (Fig. 1b). The separation of the peaks even in absence of significant mass transport discloses restrictions for reversible charge transfer, while the mirror symmetric voltammogram indicates immediate readiness of the adlayer for releasing the captured electron into the electric circuit upon the potential scan reversal, i.e. a behavior typical to electric capacitor. The corresponding capacitance C_a in the Faradaic branch of the equivalent circuit of electrochemically reversible upd was found with stationary and potentiodynamic electrochemical impedance spectroscopy in various reversible upd processes on metal substrates (Pb, Cu, Bi, Ag upd on gold, [26–28], Cu upd on Pd [29], etc.). The capacitance C_a results from oscillation of metal adatom coverage at ac probing [26, 30, 31]. C_a is typically much higher than the double layer capacitance C_{dl}. The name 'pseudocapacitance' is often used in literature for distinguishing C_a from 'true' capacitance C_{dl} of the double layer. Despite the C_a originates from the electrochemical reaction and belongs to Faradaic branch of the equivalent circuit, this pseudocapacitance is, nevertheless, a true capacitance in terms of frequency response analysis and should not be mixed with 'pseudocapacitances' which have been derived lately from CV and chronopotentiometry in a great number of publications about supercapacitors. The latter 'pseudocapacitances' are usually not capacitances in terms of frequency response analysis and the use of Farad unit is inappropriate for their characterization (a detailed discussion of this issue was presented in [32]).

Metal upd on chalcogens and on metal chalcogenides, contrary to the electrochemically reversible upd, tend to the voltammetric profile of the kind shown in Fig. 1b [26]. No reverse reaction proceeds in this case at the potential of the upd peak, so keeping the system at the potential of upd in the stationary state results not only in zero direct current response of the upd, but also in impossibility of obtaining any alternating current response of either forward or back reaction. That is why impedance spectrum has to be acquired in the potentiodynamic mode with inevitable truncation of low frequencies to provide sufficiently high scan rate. The other consequence of nonexistence of equilibrium between electrochemically irreversible forward and back reactions is the complexity of the underpotential shift ΔE_{upd} measurement in such systems [9, 33]. When the quasiequilibrium potential shown by vertical dashed line on the right in Fig. 1b is not well defined as a boundary between cathodic and anodic peaks in CV, it can be more accurately obtained as intercept of potential dependences of inverse charge transfer resistances of forward and back reactions derived with potentiodynamic electrochemical impedance spectroscopy (PDEIS) [9]. Peculiarities of PDEIS application for characterization of nonstationary systems were discussed in [26].

Underpotential shift and adlayer-substrate interaction

The underpotential shift ΔE_{upd} characterizes favorability of adatoms deposition on a foreign substrate compared to the deposition on a same metal substrate and thus may serve as a merit of metal-substrate (M-S) interaction strength [6]. ΔE_{upd} is determined by several factors [34], which are often complex to calculate: binding energies in the adlayer and between adatoms and the substrate, the influence of local surface defects of the substrate, the effects of solvent and anions. Despite complexity of ΔE_{upd} prediction, some empirical correlations were found between ΔE_{upd} and characteristics of the deposit and substrate. For instance, the underpotential shift in metal upd on metal typically shows correlation with differences of work functions of the substrate and the deposited metal [1]. On the contrary, no correlation with the differences of work functions was observed in metal upd on tellurium [9] (Fig.2a). Alternatively, the underpotential shift in metal upd on tellurium shows correlation with free energy of metal telluride formation [9] (Fig.2b). The latter correlation is the indication of metal-chalcogen covalent interaction effect in metal adlayer growth on tellurium.

Besides the covalent adatom-substrate bonding, electron energy band structure of a nonmetallic substrate affects the upd shift, e.g. no electrodeposition of metal adatoms on a wide-bandgap semiconductor p-selenium was observed in the potential region of the expected upd under dark condition; however, the electrodeposition proceeds on illuminated p-Se and the photoelectrochemically deposited adlayer gives characteristic oxidation peak in the anodic scan [35]. Underpotential shift in upd on nanoparticles of CdS, CdSe and some other chalcogenides is controlled by LUMO energy which is dependent on the semiconductor nanoparticle size, so the upd appears to be an unusual means for probing energy band structure of nanostructured materials [12]. Anodic

oxidation of Cd adlayers on *n*-type CdSe and CdS is hindered by blocking of anodic current on electrode-electrolyte interface.
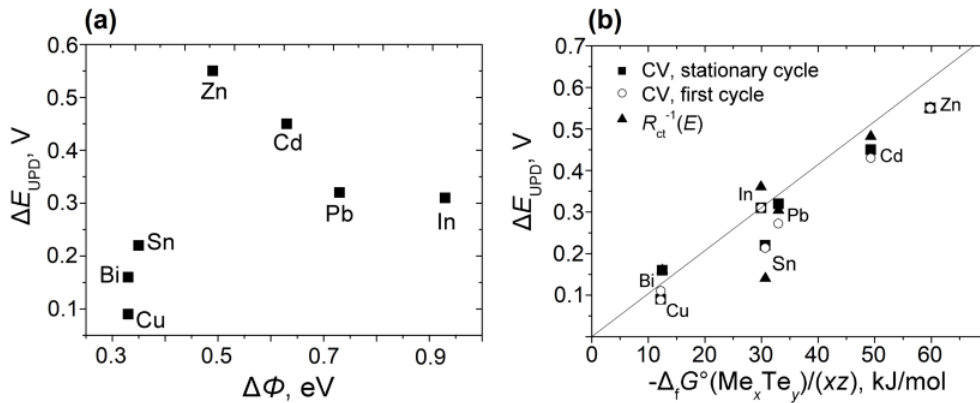

Fig. 2 Underpotential shift ΔE_{upd} for different metals on Te plotted against (a) work function difference of Te and metal, and (b) Gibbs free energy of metal telluride formation.

Fig. 3 illustrates role of the chalcogen atom in lead chalcogenide in upd behavior. The anodic to cathodic peak separation increases in the row PbTe-PbSe-PbS, which indicates the increasing irreversibility of the upd process and also partial suppression of the upd and adlayer anodic oxidation on PbS. The electrochemical irreversibility of the upd increases likely due to the chemical bond ionic character increase in the chalcogenides series.
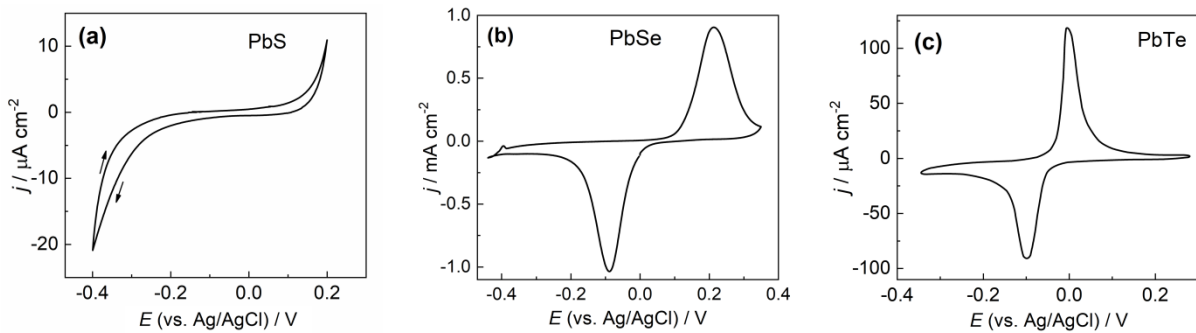

Fig. 3 Typical voltammetric profiles of Pb upd on (a) PbS, (b) PbSe, and (c) PbTe

Ionic compounds such as oxides are not prone to acquire metal adlayers at underpotential and this provides selective upd on chalcogenide component of chalcogenide-oxide heterostructures, which is considered further. The electrochemical irreversibility of the upd of the kind shown in Fig 3b is the indication of restricted electron transfer between metal adatoms and the chalcogenide support, and the restriction favors the use of upd as electrochemical probe for examination of energy band structure variation of the chalcogenide with particle size.

Pb_ad on Bi$_2$Te$_3$ vs. Pb_ad on Te

Lead upd on bismuth telluride and on tellurium proceed in the same potential region (Fig. 4) [36–38], but the cathodic part of voltammetric profile of the upd on tellurium transforms from a single peak to a two-humped structure in continuous cycling. The variability of the cathodic branch of voltammetric profile in upd on tellurium is due to adlayer gradual chemical interaction with tellurium and the corresponding gradual transition from upd on tellurium to upd on telluride in continuous cycling. The underpotential deposition of metal adatoms was found to be an efficient probe for disclosure of chemical state of surface layer of tellurium atoms in the substrate, which was helpful for detection of bismuth telluride contamination by elemental tellurium in electrodeposition.
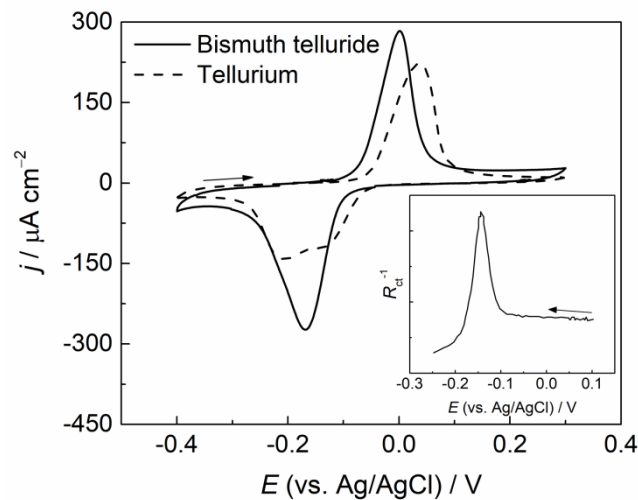

Fig. 4 Cyclic voltammograms of tellurium (dashed) and Bi$_2$Te$_3$ (solid) electrodes in the potential ranges of Pb upd from 10 mM Pb(NO$_3$)$_2$, 0.1 M KNO$_3$, 10 mM HNO$_3$ electrolyte solution. dE/dt = 50 mV·s^{-1}. The current was normalized for real surface area. Insert: inverse charge transfer resistance of the upd as a function of Bi$_2$Te$_3$ electrode potential.
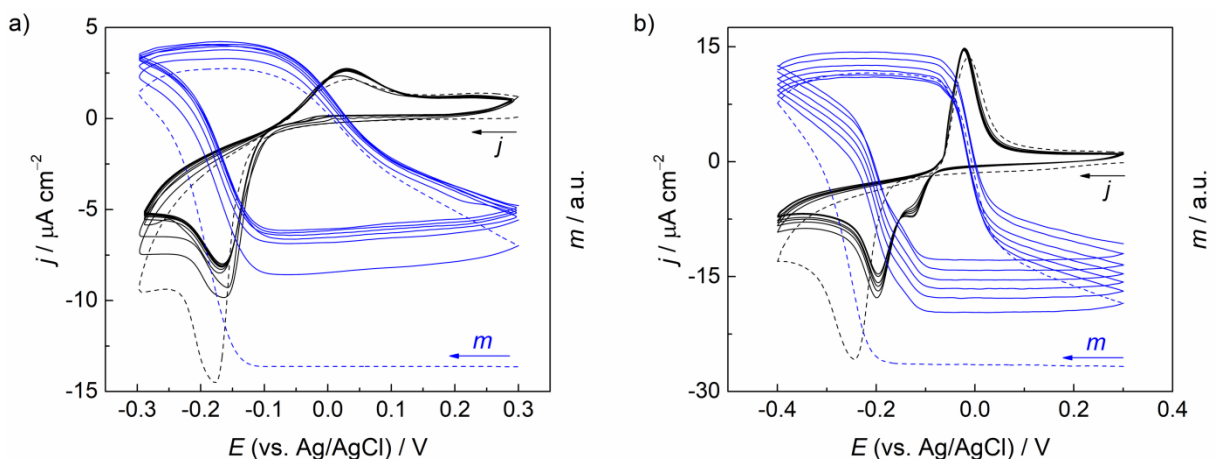

Fig. 5 Evolution of voltammetric profiles (j) of Pb adlayer cathodic deposition and anodic oxidation and cyclic changes of mass (m) in Pb upd on (a) bare Bi$_2$Te$_3$ and (b) Te. Electrolyte: 10 mM Pb(NO$_3$)$_2$, 1 mM HNO$_3$, 0.1M KNO$_3$; the first cycles are shown by dashed lines. dE/dt=10mV s^{-1}

Nanoparticles of elemental tellurium which can be coelectrodeposited with bismuth telluride, especially at high Te(IV):Bi(III) atomic ratio in electrolyte solution [11], are indistinguishable from Bi_2Te_3 in XRD analysis [37, 38]. As the latter is typically used to prove phase composition of the electrodeposits, the undetectable contamination by elemental tellurium is a potential catch in the electrochemical preparation of Bi_2Te_3-based thermoelectric materials. Fortunately, the electrochemistry of metal adlayers provides an efficient procedure for disclosure of elemental tellurium under conditions of electrodeposition [37]. The detection of elemental Te codeposition exploits peculiarities of voltammetric profiles variation at continuous cycling of lead upd on bare Bi_2Te_3 (Fig. 5a) and on elemental Te (Fig. 5b). The first cycles of the upd are hardly distinguishable on both substrates, but a characteristic difference appears in further cycles as the additional cathodic peak before the main peak in upd on tellurium and the characteristic peak increases with each cycle (Fig. 5b). Though Pb upd on bare Bi_2Te_3 is also not fully reversible (Fig. 5a), its voltammetric profile just scales down to slightly lower current density showing no additional peaks. Some irreversible mass increase in first cycles stabilizes leading to reversible mass changes resulting from adlayer deposition and dissolution in further cycles on Bi_2Te_3. Contrary to this evolution, the mass increase in Pb upd on Te progresses with each cycle. Though main part of Pb adlayer dissolves from the electrode upon anodic oxidation, some oxidized Pb adatoms form nuclei of PbTe on Te surface, so that the upd in the following cycles proceeds both on the remaining tellurium surface and on PbTe nuclei, the potential of the emerging cathodic peak corresponds perfectly to the potential of Pb upd peak on PbTe [36]. The growing peak of Pb upd on PbTe under continuous cycling was found to be a convenient indicator of Bi_2Te_3 contamination by elemental tellurium and this helped to optimize conditions of electrodeposition of individual Bi_2Te_3 and multicomponent nanostructures based on Bi_2Te_3 [11, 37].

Chalcogenide particle size effects

Besides chemical state of the chalcogen atoms on a substrate surface, the chalcogenide particle size is a significant factor for electron transfer between chalcogenide nanoparticle and metal ions in the upd. Size effects in metal upd on metal chalcogenides were studied in greater detail with the use of typical quantum dot chalcogenides CdS and CdSe [12, 13] and partly PbSe.

Cd upd on CdS and CdSe were first applied in the electrochemical atomic layer epitaxy (deposition) (ECALE/E-ALD [20, 39–41]) of the chalcogenides, although the publications about ECALE and E-ALD presented typically just cyclic voltammograms of the first steps of the intermittent deposition of metal and chalcogen atomic layers in the ECALE/E-ALD procedures and lacked information about electrochemistry of metal adlayer on chalcogenide.

Effect of CdS and CdSe particle size in the upd of Cd upd was examined with the chalcogenide particle size control by heating at different temperature of chemical bath deposited (CBD) films [13]

and also QD films electrophoretically deposited from colloidal solution of QDs of different size [12]. QD sizes in both types of the nanostructured films were derived from optical spectra.

Figure 6 shows cyclic voltammograms and inverse charge transfer resistance R_{ct}^{-1} potentiodynamic profiles of cadmium upd on the CBD CdS and CdSe films. The latter dependences obtained by analysis of PDEIS spectra characterize kinetics of the upd (R_{ct}^{-1} is proportional to electrochemical reaction rate constant). Fig. 6c,d insets show the equivalent electric circuit which fitted well to the PDEIS data in the potential range of the upd. The absence of diffusion impedance in the circuit corresponds to negligible contribution of mass transport to the PDEIS data; however, this does not necessarily exclude mass transport in the upd, as the low frequencies which normally give information about diffusion had to be truncated during impedance spectra acquisition in the potentiodynamic mode. The most significant feature in the potentiodynamic profiles of both the current and R_{ct}^{-1} is their clear dependence on the QD size – the smaller are the chalcogenide QDs the lower is the underpotential shift. The size effects in the upd on chalcogenide QDs are somewhat similar to those in upd on small metal particles [42–44], but metal particles show size effects at much higher size.
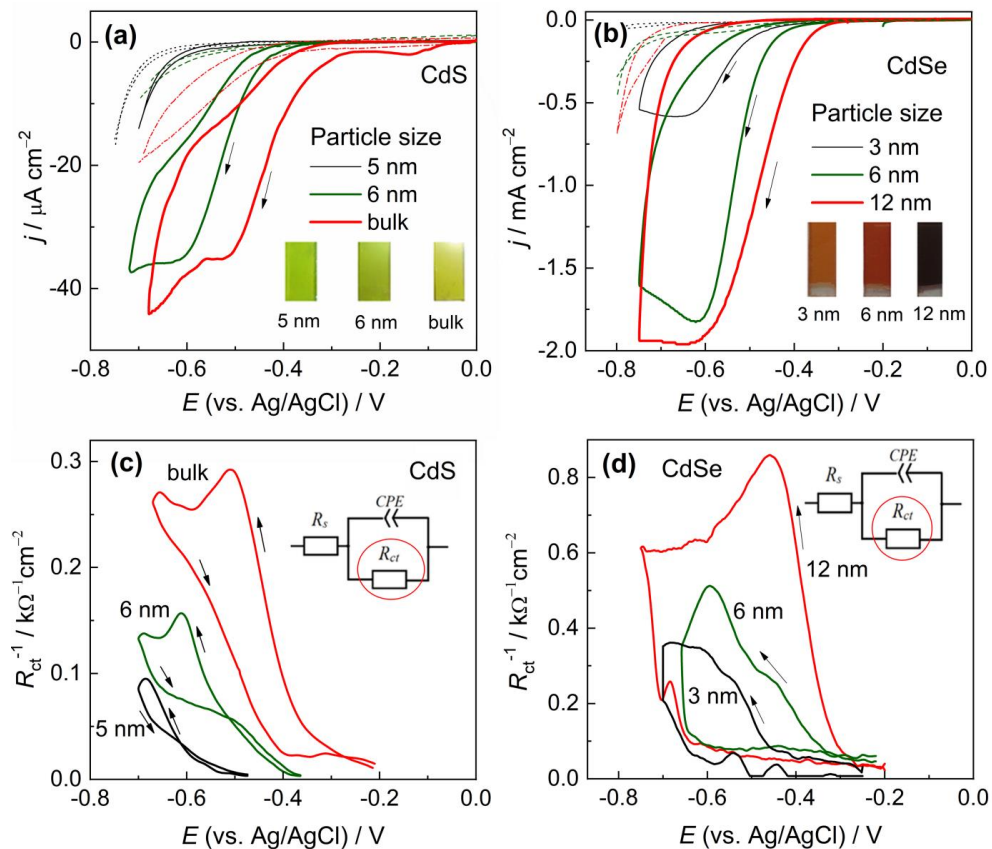

Fig. 6 (a), (b) CVs and (c), (d) potentiodynamic profiles of reciprocal charge transfer resistance R_{ct}^{-1} of Cd upd on CdS and CdSe CBD films with particles of different size. Electrolyte: 10 mM $CdSO_4$ + 0.1M Na_2SO_4 (solid), dotted lines correspond to blank 0.1M Na_2SO_4
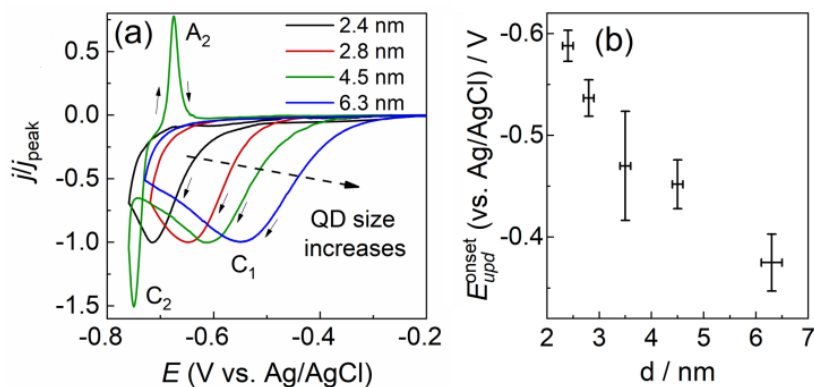
Fig. 7 (a) Normalized CVs for CdSe EPD QD films with different QD size in 10 mM CdSO$_4$ + 0.1M Na$_2$SO$_4$ and (b) onset potentials of Cd upd vs. CdSe QD size

Figure 7 presents size effects in cadmium upd (peaks C$_1$) on electrophoretically deposited (EPD) films of CdSe QDs of different size [12]. The QDs were synthesized by a method described in [45] which gives much narrower size distribution compared to chemical bath deposition and this resulted in the greater perfectness of the size effects in the upd. The figure shows also potentials of bulk Cd cathodic deposition (C$_2$) and anodic oxidation (A$_2$) for comparison with the potentials of upd, the latter proceeds both in the region of bulk metal anodic oxidation and below reversible potential E(Cd^{2+}/Cd). The upd competes efficiently with bulk phase electrodeposition in a narrow region below E(Cd^{2+}/Cd) due to overpotential of metal phase nucleation.

Figure 8a shows in terms of absolute electrode potential the correspondence of cadmium upd onset potential on CdSe to LUMO energy levels of CdSe QDs. Based on comparison of QD size effect on LUMO level and on the upd onset potential, the upd potential dependence on QD size was explained in [12] as the effect of the charge transfer control by the size-dependent position of LUMO level: the decrease in QD size results in the upward LUMO shift, so the electron transfer from electrode to metal cation via the LUMO energy level proceeds at more negative electrode potential.
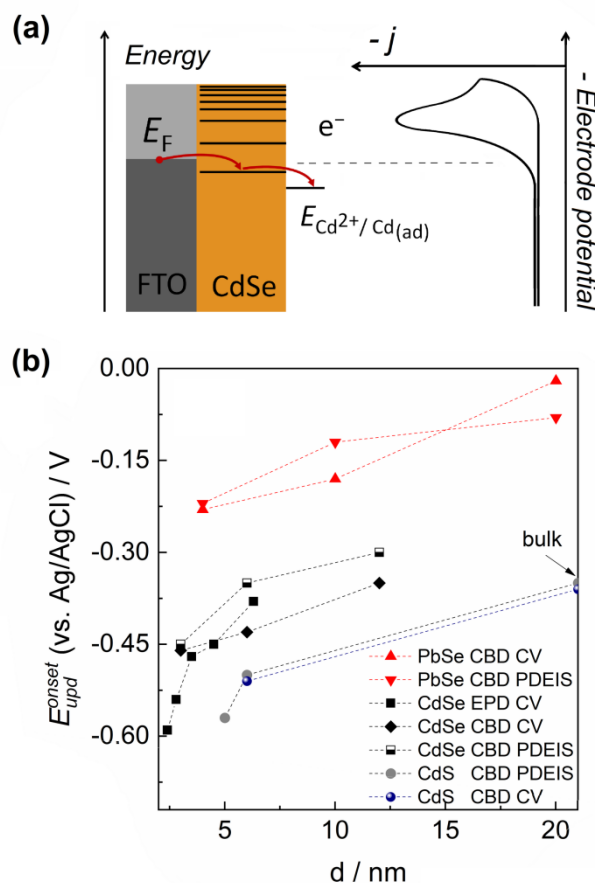
Fig. 8 (a) Energy diagram proposed for charge transfer in upd process on a chalcogenide nanoparticle. (b) Onset potentials of upd (derived from CV and PDEIS) vs. particle size for different chalcogenides. The potentials are shown for Cd upd on different cadmium chalcogenides and Pb upd on PbSe

Figure 8b summarizes size effect on upd onset potential on different chalcogenides. These dependences can help to better understand cathodic reduction reactions on chalcogenide nanoparticles, not just upd; e.g. electrochemical corrosion of $A^{II}B^{VI}$ particles which proceeds via formation of adatoms of metal A [46]. Also, the size-dependent upd appears to be an interesting new means of evaluation of the conduction band position in chalcogenide nanomaterials [12].

Electroactive surface area measurement

Electrochemical adsorption of hydrogen on Pt has been for long time the basic method of real surface area measurement of platinum electrodes, the electrochemical adsorption of oxygen on gold is a common method of gold electrodes real surface area measurement [47]. Also, Pb [48, 49], Cu [50], and Hg [51] upd and oxidation of adsorbed CO layer [52] have been used to measure real surface area of some metal electrodes. The simple principle behind the surface area measurement is that adlayer oxidation/deposition charge is proportional to the area. The similar approach has provided measurement of the electroactive surface area of metal chalcogenides by underpotential deposition of metals. In work [53], the evolution of PbSe film roughness was estimated in the course of electrodeposition. The electrochemical deposition was terminated at different time and Pb adlayer

oxidation charge was measured. Fig. 9 shows the resulting dependence of the adlayer oxidation charge on deposition time. The figure shows that PbSe surface area grows fast and almost linearly with time at very beginning of the deposition and the growth slows down afterwards. The real surface area became equal to geometric area by approx. third second and showed a 13-fold excess at 600 seconds of deposition.
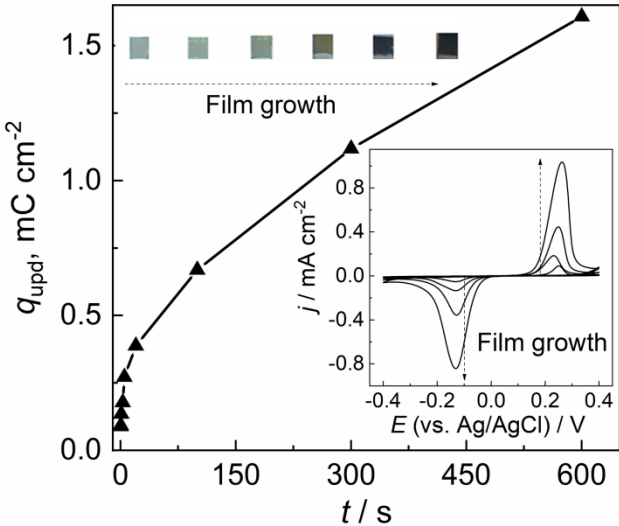

Fig. 9 The Pb adlayer oxidation charge per geometric surface area vs. PbSe deposition time. The inset shows CVs of PbSe film electrodes in Pb^{2+}-containing electrolyte (deposition time 0.5 s, 5 s, 100 s, 600 s). Images of PbSe films at different stages of electrodeposition are shown as a row of rectangles on the top
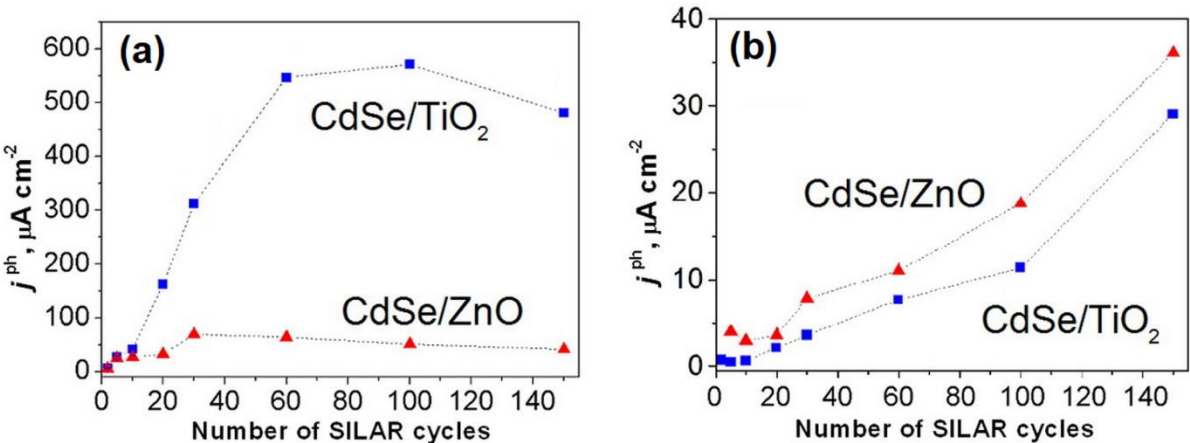

Fig. 10 Sensitized photocurrent on $CdSe/TiO_2$ (1) and $CdSe/ZnO$ (2) nanostructured electrodes normalized for (a) geometric surface area and (b) electroactive surface area of CdSe sensitizer component of the heterostructurs at variable number of SILAR deposition cycles [14].

The measurement of electroactive surface area of metal chalcogenides by metal upd is especially helpful in investigations of chalcogenide heterostructures in which the other component is incapable of acquiring metal adlayer at underpotential, so the upd proceeds selectively on one component of the heterostructure and provides information about electroactive surface area of that particular component. Fig. 10 shows how this method works in the investigation of spectral sensitizing of wide-bandgap oxides by CdSe nanoparticles [14]. The photocurrent sensitized by CdSe passes maximum with the increase in number of CdSe deposition cycles of successive ionic layer adsorption and reaction (SILAR) technique when the current is referred to geometric surface area (Fig. 10a) and this may result in a wrong conclusion about variation of CdSe sensitizing activity with number of SILAR cycles. Renormalization of the same photocurrent data for the electroactive surface area of the sensitizer component provided with the application of cadmium selective upd on CdSe gave an entirely different dependence of the photocurrent shown in Fig. 10b. The figure shows that the sensitizing activity of a unit surface area of the sensitizer in fact increased with number of SILAR cycles even in the region of the photocurrent decrease of Fig. 10a. The selective upd provides in tasks of this kind a unique opportunity of deriving specific characteristics of one component of multicomponent system from measurements applied on the whole system.

From adlayers to interlayers

Bismuth telluride is an example of chalcogenide with layered structure. Bi_2Te_3 crystal consists of Te-Bi-Te-Bi-Te quintuples connected to each other by weak van der Waals bonds. Metal atoms can be inserted between the quintuples at van der Waals planes. The stable form of the inserted bismuth is atomic bilayer – a combination of two adlayers Bi_{ad} which interact with bismuth telluride on the one side and form Bi-Bi bonds on the other side [11, 54]. The product of bismuth bilayer insertion into bismuth telluride $(Bi_2)_m(Bi_2Te_3)_n$ appears as additive to bismuth telluride at bismuth telluride electrodeposition from electrolyte with high Bi(III):Te(IV) atomic ratio [11]. Figure 11 shows typical voltammetric signatures of $(Bi_2)_m(Bi_2Te_3)_n$ at electrochemical conditions of codeposition with bismuth telluride. The potential region of the anodic peak attributed to bismuth bilayer anodic oxidation overlaps with the region of Bi_{ad} anodic oxidation on Bi_2Te_3 at moderate Bi(III):Te(IV) atomic ratio and shifts negatively with Bi(III) concentration increase (Fig. 11), i.e. in the opposite direction to the one expected for Nernstian shift of bulk bismuth anodic peak. The difference in Bi oxidation potentials and the opposite effect of Bi(III) concentration on the potentials of the both anodic peaks helps to distinguish them electrochemically.
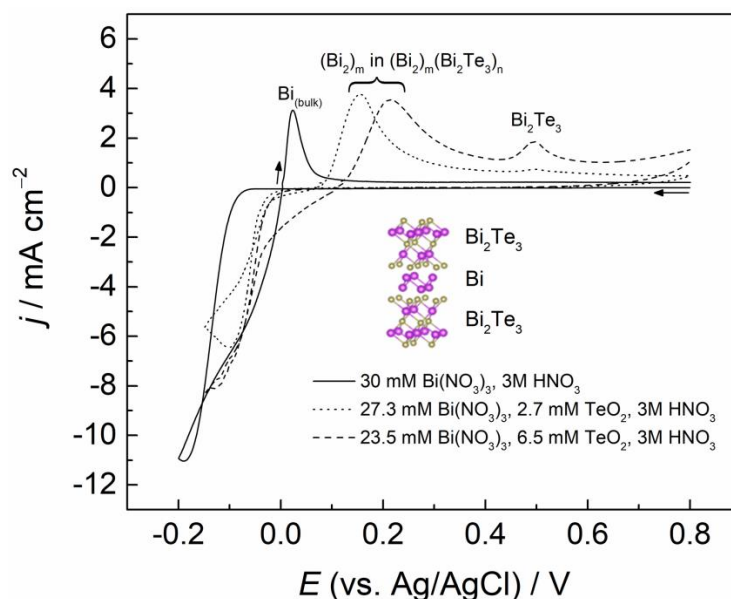
Fig. 11 Cyclic voltammograms of stainless steel electrode in the electrolytes with different Bi(III):Te(IV) ratio. dE/dt = 50 mV·s^{-1}. The current was normalized for real surface area. Inset shows the structure of $(Bi_2)_m(Bi_2Te_3)_n$

The technique for individual $(Bi_2)_m(Bi_2Te_3)_n$ electrodeposition was developed [11] based on pulsed potentiostatic control of two controlled potentials – the potentials of electrodeposition and electrochemical refinement. The refinement was applied after electrodeposition in each period at the potential which corresponded to a very beginning of bismuth bilayer anodic oxidation wave. Periodic switching between the deposition and refinement potentials helped to obtain the superlattices with general formula $(Bi_2)_m(Bi_2Te_3)_n$ and variable bismuth content dependent on electrolyte concentration. The products were identified with various methods and characterized electrochemically [11]. Interestingly, the potentiostatic treatment of $(Bi_2)_m(Bi_2Te_3)_n$ at the potential of bismuth bilayer anodic oxidation resulted in the product close to bismuth telluride by atomic composition but having an expanded structure, which could be of interest for further design of complex nanostructured materials based on bismuth telluride.

Conclusions

Cathodic underpotential deposition of metal adlayer on metal chalcogenide is the electrochemically irreversible surface limited reaction, hence the cathodic deposition of the adlayer and its anodic oxidation proceed in poorly overlapping or not overlapping potential intervals. The irreversibility of the upd increases in the row from tellurides to selenides and further to sulfides, additionally the upd is significantly hindered on sulfides, probably due to greater ionicity of Me-S bond and wider bandgap.

The underpotential shift on chalcogenide nanoparticles increases with particle size. Size effect in Cd upd on CdSe which was investigated in a greater detail results from size dependence of LUMO

energy and its correspondence to the onset potential of upd. Due to the correlation of the upd onset potential and LUMO energy, the onset potential of cadmium upd appears to be an unusual electrochemical means of CdSe quantum dot size measurement, and this may be of practical use in systems with complications for in situ optical measurement of QD size.

Upd on chalcogenides has been applied as a means of measurement of electroactive surface area of chalcogenide electrodes. Especially advantageous is the application of this method for the surface area measurement of chalcogenide component of heterostructures with the other component being incapable of providing upd, such as CdSe-TiO$_2$, CdSe-ZnO, etc.

Metal adlayers on chalcogenides were found to be stable against reaction with substrate. In contrast, metal adlayer deposited on chalcogen tend to react with substrate upon prolonged cycling of the adlayer cathodic deposition and anodic oxidation. This effect was applied for detection of trace amount of tellurium on bismuth telluride surface by lead upd which showed Pb upd on PbTe voltammetric signature emergence in the continuous cycling in presence of tellurium.

An interesting further task in the electrochemistry of adlayers refers to their electrochemical incorporation inside layered chalcogenides and thus forming superlattice structure. In particular, bismuth-bismuth telluride superlattices with bismuth interlayers can be obtained by electrodeposition in pulse potentiostatic mode with control of two potentials.

References

1. Kolb DM, Przasnyski M, Gerischer H (1974) Underpotential deposition of metals and work function differences. J Electroanal Chem Interfacial Electrochem 54:25–38. https://doi.org/10.1016/S0022-0728(74)80377-3

2. Adžić RR (1979) Electrocatalysis on Surfaces Modified by Foreign Metal Adatoms. Isr J Chem 18:166–181. https://doi.org/10.1002/ijch.197900021

3. Conway BE (1984) Electrochemical surface science: The study of monolayers of ad-atoms and solvent molecules at charged metal interfaces. Prog Surf Sci 16:1–137. https://doi.org/10.1016/0079-6816(84)90008-X

4. Kokkinidis G (1986) Underpotential Deposition and Electrocatalysis. J Electroanal Chem interfacial Electrochem 201:217–236. https://doi.org/10.1016/0022-0728(86)80051-1

5. Herrero E, Buller LJ, Abruña HD (2001) Underpotential deposition at single crystal surfaces of Au, Pt, Ag and other materials. Chem Rev 101:1897–1930. https://doi.org/10.1021/cr9600363

6. Oviedo OA, Reinaudi L, Garcia SG, Leiva EPM (2016) Underpotential Deposition: from Fundamentals and Theory to Applications at the Nanoscale. In: Scholz F (ed) Monographs in Electrochemistry. Springer, Berlin

7. Scholz F, Leiva EPM (2018) Moïse Haïssinsky: The Discoverer of Underpotential Deposition. ChemElectroChem 5:849–854. https://doi.org/10.1002/celc.201700770

8. Streltsov EA, Osipovich NP, Ivanou DK (2005) Metal underpotential deposition on tellurium and selenium. Electrochemical preparation of metal chalcogenide films and nanostructures. In: Norris CP (ed) Focus on Surface Science Research. Nova Science Publ, New York, pp 1–69

9. Chulkin PV, Aniskevich YM, Streltsov EA, Ragoisha GA (2015) Underpotential shift in electrodeposition of metal adlayer on tellurium and the free energy of metal telluride formation. J Solid State Electrochem 19:2511–2516. https://doi.org/10.1007/s10008-015-2831-x

10. Bouroushian M (2010) Electrochemistry of Metal Chalcogenides. In: Scholz F (ed) Monographs in Electrochemistry. Springer, Berlin

11. Bakavets A, Aniskevich Y, Yakimenko O, Jo JH, Vernickaite E, Tsyntsaru N, Cesiulis H, Kuo LY, Kaghazchi P, Ragoisha G, Myung ST, Streltsov E (2020) Pulse electrodeposited bismuth-tellurium superlattices with controllable bismuth content. J Power Sources 450:227605. https://doi.org/10.1016/j.jpowsour.2019.227605

12. Aniskevich Y, Antanovich A, Prudnikau A, Artemyev MV, Mazanik AV, Ragoisha G, Streltsov EA (2019) Underpotential Deposition of Cadmium on Colloidal CdSe Quantum Dots: Effect of Particle Size and Surface Ligands. J Phys Chem C 123:931–939. https://doi.org/10.1021/acs.jpcc.8b10318

13. Aniskevich YM, Malashchonak MV, Chulkin PV, Ragoisha GA, Streltsov EA (2016) Cadmium underpotential deposition on CdSe and CdS quantum dot films: size dependent underpotential shift. Electrochim Acta 220:493–499. https://doi.org/10.1016/J.ELECTACTA.2016.10.132

14. Malashchonak MV, Streltsov EA, Ragoisha GA, Dergacheva MB, Urazov KA (2016) Evaluation of electroactive surface area of CdSe nanoparticles on wide bandgap oxides (TiO$_2$, ZnO) by cadmium underpotential deposition. Electrochem commun 72:176–180. https://doi.org/10.1016/J.ELECOM.2016.10.004

15. Gregory BW, Stickney JL (1991) Electrochemical atomic layer epitaxy (ECALE). J

Electroanal Chem Interfacial Electrochem 300:543–561. https://doi.org/10.1016/0022-0728(91)85415-L

16. Innocenti M, Pezzatini G, Forni F, Foresti ML (2001) CdS and ZnS Deposition on Ag(111) by Electrochemical Atomic Layer Epitaxy. J Electrochem Soc 148:C357–C362. https://doi.org/10.1149/1.1360208

17. Öznülüer T, Erdoğan I, Şişman I, Demir Ü (2005) Electrochemical atom-by-atom growth of PbS by modified ECALE method. Chem Mater 17:935–937. https://doi.org/10.1021/cm048246g

18. Banga D, Perdue B, Stickney J (2014) Electrodeposition of a PbTe/CdTe superlattice by electrochemical atomic layer deposition (E-ALD). J Electroanal Chem 716:129–135. https://doi.org/10.1016/j.jelechem.2013.08.009

19. Shen S, Zhang X, Perdue B, Stickney JL (2018) Formation of CdS using electrochemical atomic layer deposition (E-ALD) and successive ionic layer adsorption reaction (SILAR). Electrochim Acta 271:19–26. https://doi.org/10.1016/j.electacta.2018.03.119

20. Colletti LP, Flowers Jr BH, Stickney JL (1998) Formation of Thin Films of CdTe, CdSe, and CdS by Electrochemical Atomic Layer Epitaxy. J Electrochem Soc 145:1442–1449. https://doi.org/10.1149/1.1838502

21. Pezzatini G, Caporali S, Innocenti M, Foresti ML (1999) Formation of ZnSe on Ag(111) by electrochemical atomic layer epitaxy. J Electroanal Chem 475:164–170. https://doi.org/10.1016/S0022-0728(99)00347-2

22. Venkatasamy V, Mathe MK, Cox SM, Happek U, Stickney JL (2006) Optimization studies of HgSe thin film deposition by electrochemical atomic layer epitaxy (EC-ALE). Electrochim Acta 51:4347–4351. https://doi.org/10.1016/j.electacta.2005.12.012

23. Forni F, Innocenti M, Pezzatini G, Foresti ML (2000) Electrochemical aspects of CdTe growth on the face (111) of silver by ECALE. Electrochim Acta 45:3225–3231. https://doi.org/10.1016/S0013-4686(00)00426-6

24. Scholz F, Meyer B (1994) Electrochemical solid state analysis: State of the art. Chem Soc Rev 23:341–347. https://doi.org/10.1039/CS9942300341

25. Doménech-Carbó A, Labuda J, Scholz F (2013) Electroanalytical chemistry for the analysis of solids: Characterization and classification (IUPAC technical report). Pure Appl Chem 85:609–631. https://doi.org/10.1351/PAC-REP-11-11-13

26. Ragoisha GA (2015) Potentiodynamic Electrochemical Impedance Spectroscopy for Underpotential Deposition Processes. Electroanalysis 27:855–863. https://doi.org/10.1002/elan.201400648

27. Garland JE, Assiongbon KA, Pettit CM, Emery SB, Roy D (2002) Kinetic analysis of electrosorption using fast Fourier transform electrochemical impedance spectroscopy: Underpotential deposition of Bi^{3+} in the presence of coadsorbing ClO^{4-} on gold. Electrochim Acta 47:4113–4124. https://doi.org/10.1016/S0013-4686(02)00437-1

28. Cesiulis H, Tsyntsaru N, Ramanavicius A, Ragoisha G (2016) The study of thin films by electrochemical impedance spectroscopy. In: Tiginyanu I, Topala P, Ursaki V (eds) Nanostructures and thin films for multifunctional applications. NanoScience and Technology, Springer, Cham, pp 3–42. https://doi.org/10.1007/978-3-319-30198-3_1

29. Huang M, Henry JB, Fortgang P, Henig J, Plumeré N, Bandarenka AS (2012) In depth analysis of complex interfacial processes: In situ electrochemical characterization of deposition of atomic layers of Cu, Pb and Te on Pd electrodes. RSC Adv 2:10994–11006. https://doi.org/10.1039/c2ra21558f

30. B E Conway (1999) Electrochemical supercapacitors : scientific fundamentals and technological applications. Plenum Publishers, New York

31. Bondarenko AS, Ragoisha GA, Osipovich NP, Streltsov EA (2005) Potentiodynamic electrochemical impedance spectroscopy of lead upd on polycrystalline gold and on selenium atomic underlayer. Electrochem commun 7:631–636. https://doi.org/10.1016/J.ELECOM.2005.04.001

32. Ragoisha GA, Aniskevich YM (2016) arXiv:1604.08154. https://arxiv.org/pdf/1604.08154

33. Aniskevich YM, Chulkin PV, Streltsov EA, Ragoisha GA (2015) Underpotential deposition of metal on tellurium and the free energy of metal telluride formation. In: Physics, Chemistry and Applications of Nanostructures. World Scientific, pp 299–302. https://doi.org/10.1142/9789814696524_0074

34. Oviedo OA, Mayer CE, Staikov G, Leiva EPM, Lorenz WJ (2006) Low-dimensional metallic nanostructures and their electrochemical relevance: Energetics and phenomenological approach. Surf Sci 600:4475–4483. https://doi.org/10.1016/j.susc.2006.07.016

35. Ragoisha GA, Streltsov EA, Rabchynski SM, Ivanou DK (2011) Cadmium cathodic deposition on polycrystalline p-selenium: Dark and photoelectrochemical processes. Electrochim Acta 56:3562–3566. https://doi.org/10.1016/j.electacta.2010.12.042

36. Ragoisha G., Bondarenko A., Osipovich N., Streltsov E. (2004) Potentiodynamic electrochemical impedance spectroscopy: lead underpotential deposition on tellurium. J Electroanal Chem 565:227–234. https://doi.org/10.1016/J.JELECHEM.2003.10.014

37. Bakavets AS, Aniskevich YM, Ragoisha GA, Streltsov EA (2018) Underpotential deposition of lead onto Bi_2Te_3 / Te heterostructures. Electrochem. commun. 94:23–26. https://doi.org/10.1016/j.elecom.2018.07.018

38. Bakavets AS, Aniskevich YM, Ragoisha GA, Streltsov EA (2017) Bismuth and lead underpotential deposition on bismuth telluride: new insights into the electrochemical synthesis of bismuth telluride and evaluation of real surface area. J Belarusian State Univ Chem 1:3–13

39. Lister TE, Stickney JL (1996) Formation of the first monolayer of CdSe on Au(111) by electrochemical ALE. Appl Surf Sci 107:153–160. https://doi.org/10.1016/S0169-4332(96)00488-6

40. Colletti LP, Teklay D, Stickney JL (1994) Thin-layer electrochemical studies of the oxidative underpotential deposition of sulfur and its application to the electrochemical atomic layer epitaxy deposition of CdS. J Electroanal Chem 369:145–152. https://doi.org/10.1016/0022-0728(94)87092-6

41. Gichuhi A, Boone BE, Demir U, Shannon C (1998) Electrochemistry of S adlayers at underpotentially deposited Cd on Au(111): Implications for the electrosynthesis of high-quality CdS thin films. J. Phys. Chem. B 102:6499–6506

42. Zhou YG, Rees N V., Compton RG (2011) Nanoparticle-electrode collision processes: The underpotential deposition of thallium on silver nanoparticles in aqueous solution. ChemPhysChem 12:2085–2087. https://doi.org/10.1002/cphc.201100282

43. Campbell FW, Zhou YG, Compton RG (2010) Thallium underpotential deposition on silver nanoparticles: Size-dependent adsorption behaviour. New J Chem 34:187–189. https://doi.org/10.1039/b9nj00669a

44. Campbell FW, Compton RG (2010) Contrasting underpotential depositions of lead and cadmium on silver macroelectrodes and silver nanoparticle electrode arrays. Int J Electrochem Sci 5:407–413

45. Shen H, Wang H, Tang Z, Niu JZ, Lou S, Du Z, Li LS (2009) High quality synthesis of

monodisperse zinc-blende CdSe and CdSe/ZnS nanocrystals with a phosphine-free method. CrystEngComm 11:1733–1738. https://doi.org/10.1039/b909063k

46. Zhao J, Holmes MA, Osterloh FE (2013) Quantum confinement controls photocatalysis: A free energy analysis for photocatalytic proton reduction at CdSe nanocrystals. ACS Nano 7:4316–4325. https://doi.org/10.1021/nn400826h

47. Trasatti S, Petrii OA (1992) Real surface area measurements in electrochemistry. J Electroanal Chem 327:353–376. https://doi.org/10.1016/0022-0728(92)80162-W

48. Kirowa-Eisner E, Bonfil Y, Tzur D, Gileadi E (2003) Thermodynamics and kinetics of upd of lead on polycrystalline silver and gold. J Electroanal Chem 552:171–183. https://doi.org/10.1016/S0022-0728(03)00181-5

49. Liu Y, Bliznakov S, Dimitrov N (2009) Comprehensive study of the application of a pb underpotential deposition-assisted method for surface area measurement of metallic nanoporous materials. J Phys Chem C 113:12362–12372. https://doi.org/10.1021/jp901536f

50. Chen D, Tao Q, Liao LW, Liu SX, Chen YX, Ye S (2011) Determining the Active Surface Area for Various Platinum Electrodes. Electrocatalysis 2:207–219. https://doi.org/10.1007/s12678-011-0054-1

51. Alia SM, Hurst KE, Kocha SS, Pivovar BS (2016) Mercury Underpotential Deposition to Determine Iridium and Iridium Oxide Electrochemical Surface Areas. J Electrochem Soc 163:F3051–F3056. https://doi.org/10.1149/2.0071611jes

52. Brett DJL, Atkins S, Brandon NP, Vesovic V, Vasileiadis N, Kucernak AR (2004) Investigation of reactant transport within a polymer electrolyte fuel cell using localised CO stripping voltammetry and adsorption transients. J Power Sources 133:205–213. https://doi.org/10.1016/j.jpowsour.2004.02.007

53. Aniskevich YM, Malashchonak MV, Bakavets AS, Ragoisha GA, Streltsov EA (2019) Determination of the Electrochemically Active Surface Area of PbSe and Bi_2Te_3 Films Using the Deposition of Lead Atoms. Theor Exp Chem 55:64–71. https://doi.org/10.1007/s11237-019-09597-3

54. Bos JWG, Zandbergen HW, Lee MH, Ong NP, Cava RJ (2007) Structures and thermoelectric properties of the infinitely adaptive series $(Bi_2)_m(Bi_2Te_3)_n$. Phys Rev B - Condens Matter Mater Phys 75:1–9. https://doi.org/10.1103/PhysRevB.75.195203